Acta Crystallographica Section D
Biological Crystallography
ISSN 0907-4449

Combined use of AFM and X-ray diffraction to analyze crystals of an engineered, domain-deleted antibody

Steven B. Larson,[a] Yu. G. Kuznetsov,[a] John Day,[a] Jiashu Zhou,[a] Scott Glaser,[b] Gary Braslawsky[b] and Alexander McPherson[a]*

[a]University of California, Irvine, Department of Molecular Biology and Biochemistry, Irvine, CA 92697-3900, USA, and [b]Biogen–IDEC, La Jolla, CA, USA

Correspondence e-mail: amcphers@uci.edu

Received 6 August 2004
Accepted 13 January 2005

A genetically engineered humanized C_H2-domain-deleted monoclonal antibody lacking any interchain-hinge disulfide bonds has been crystallized in the presence of detergent in a form suitable for X-ray diffraction analysis. The crystals were grown from 4 *M* formate along with Triton X-100 and had $P2_12_12$ space-group symmetry, with unit-cell parameters $a = 83$, $b = 224$, $c = 167$ Å. The crystals diffract to beyond 2.8 Å resolution. A disordered crystal form of larger size and more attractive habit was also grown from 4 *M* formate, but in the presence of the Anapoe series of detergents. Preliminary X-ray data, in conjunction with atomic force microscopy images, are consistent with asymmetric units consisting of two intact antibodies forming a circular dimeric ring. The crystallizing unit, which must contain a twofold axis, is a toroidal assembly of four antibodies (two dimeric rings). Competition between dimers and tetramers to enter the lattice, along with a unique kind of planar defect of packing, may be responsible for the unusually high defect density and the disorder of the X-ray diffraction pattern exhibited by the second crystal form. An approach to crystallizing proteins showing phase separation, particularly intact antibodies, that uses a preliminary detergent test set is described.

1. Introduction

HuCC49ΔCH2 is a genetically engineered antibody fragment having high affinity for the pan-carcinoma tumor antigen TAG-72, which is overexpressed on a majority of human carcinomas, including colorectal, gastric, pancreatic, lung and ovarian (Slavin-Chiorini *et al.*, 1997). HuCC49ΔCH2 is a humanized γ1 Mab in which the C_H2 domain was completely deleted and the C_H3 domain directly attached to the γ1 hinge *via* a ten-amino-acid Gly/Ser spacer. The framework and constant regions of the humanized antibody were of human origin and the complementarity-determining loops were murine.

Biosynthesis and secretion of HuCC49ΔCH2 in mammalian Chinese hamster ovary cells produced an almost equal mixture of two 122 kDa homodimeric isoforms (Mueller *et al.*, 1990; Braslawsky *et al.*, 2003). One isoform, referred to as A, contained covalent interchain disulfide bonds at heavy-chain hinge positions 239 and 242 in the Kabat numbering system (Kabat *et al.*, 1991). The quaternary structure of the second stable isoform that was investigated, B, was maintained only by non-covalent interactions through C_H3 domains. It failed to develop any interchain disulfide bonds as evidenced by the formation of a 60 kDa product consisting only of a single heavy and light chain under heated non-reducing denaturing conditions (Braslawsky *et al.*, 2003).

HuCC49ΔCH2 is of importance from a medical standpoint because of its development for radioimmunotherapy of solid tumors. C_H2-domain-deleted antibodies have serum-clearance rates in rodent models and in human clinical trials that are consistent with much smaller Mab fragments such as $F(ab')_2$. In human tumor mouse xenograft models, treatment with radiolabeled HuCC49ΔCH2 resulted in efficient tumor retention of the antibody, despite rapid serum clearance when compared with full-length CC49 IgG (Mueller *et al.*, 1990). As radioimmunotherapeutics, they address the issue of reducing certain dose-limiting toxicities, primarily bone-marrow toxicity, found with full-length IgG radiolabeled antibodies in the circulatory system and vascular pools (Mueller *et al.*, 1990; Calvo *et al.*, 1993; Slavin-Chiorini *et al.*, 1995), while maintaining efficient tumor localization.

In this paper, we describe the crystallization of the B isoform of a C_H2 domain-deleted antibody and preliminary characterization by X-ray diffraction and atomic force microscopy (AFM).

2. Materials and methods

The antibody HuCC49ΔCH2, form B, was manufactured by Biogen–Idec (La Jolla, CA, USA) and stored at a concentration of 10 mg ml^{-1} in sterile phosphate-buffered saline pH 7.2. It was subsequently concentrated to 16 mg ml^{-1} using Centricon spin concentrators (Amicon, Bedford, MA, USA). All crystallization trials, optimization and production of crystals for diffraction and AFM analysis were carried out using sitting-drop vapor-diffusion methods (reviewed by McPherson, 1999) in Cryschem plates (Hampton Research, Aliso Viejo, CA, USA). Screening was carried out using Crystal Screens I and II and Detergent Screens I, II and III (Hampton Research). Detergents for the initial trial set were from Anatrace Co. (Maumee, OH, USA). Trials were carried out at 295 K, although, where appropriate, experiments were also conducted at 277 K. Microdrops were generally 12 µl in size and reservoirs were 0.65 ml.

Table 1
Initial detergent trial set.

Detergent	CMC† (m*M*)
n-Octyl-β-D-glycopyranoside (βDG)	20
n-Octyl-β-D-thiomaltoside	20
Nananoyl-*N*-methylglucamide (MEGA-9)	25
n-Decyl-β-D-maltoside	1.8
Cyclohexyl-methyl-β-D-maltoside (CYMAL-2)	120
n-Dodecyl-α-D-maltopyranoside	0.15
Anapoe X-405‡	Not available
Triton X-100‡	0.01

† Critical micelle concentration. ‡ Final choices after optimization.

For data collection, crystals were mounted conventionally in quartz capillaries for analysis at 295 K and were frozen on loops in the cryostream for analysis at 100 K. Crystals were examined by X-ray diffraction on a laboratory R-AXIS instrument consisting of an RU-200 Rigaku rotating-anode X-ray generator fitted with Osmic mirrors with a dual image-plate detector. Analysis and data collection were also carried out at the Advanced Light Source beamline 5.0.2 at the Lawrence Berkeley National Laboratory, Berkeley, CA, USA. Data were processed using both *DENZO*/*SCALEPACK* (Otwinowski & Minor, 1997) and *d*TREK* (Pflugrath, 1999).

Atomic force microscopy (AFM) was carried out as previously described for macromolecular crystals using a Nanoscope IIIa atomic force microscope (Digital Instruments, Santa Barbara, CA, USA; Kuznetsov *et al.*, 1997; McPherson *et al.*, 2000, 2001). Crystals under growth conditions were imaged undergoing layer addition in their mother liquors in a 75 µl fluid cell, using oxide-sharpened silicon nitride tips. Growing crystals were also imaged by washing the crystals with protein-free mother liquor, which terminated growth, and then exposing the crystals to protein-free mother liquor containing 0.1% glutaraldehyde. Fixation in this way allowed imaging of molecules and aggregates adsorbed to crystal surfaces, which would otherwise have been unobservable by AFM. Images were collected in tapping mode using an oscillation frequency of about 9.2 kHz and a scanning frequency of 1 Hz. Dimensions were obtained from the height of an object above background or from center-to-center distances in crystalline arrays (Kuznetsov *et al.*, 1997).

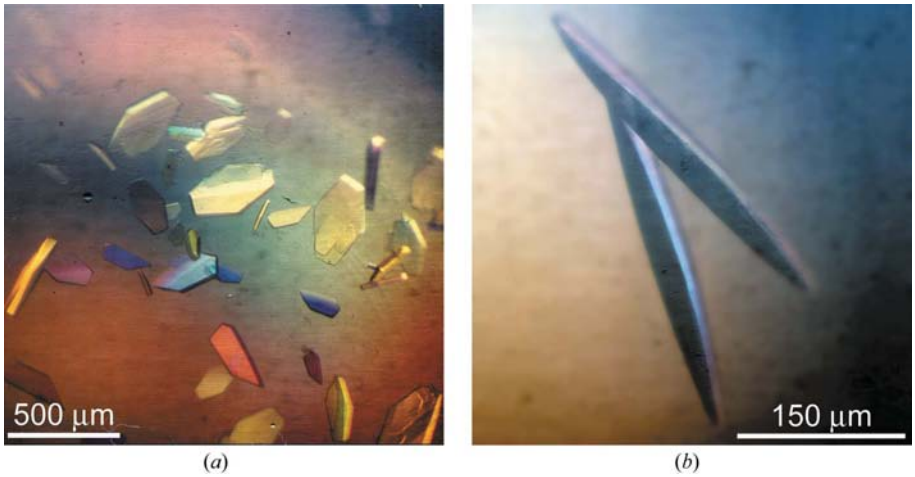

Figure 1
(*a*) Crystals of HuCC49ΔCH2, a C_H2-domain-deleted chimeric antibody grown from 4 *M* sodium formate in the presence of Anapoe X-450. (*b*) Crystals of the same antibody grown under identical conditions but using Triton X-100 as the detergent.

3. Results

Initial crystallization trials with Crystal Screens I and II at both 295 and 277 K were uniformly unsuccessful. Most of the samples, particularly those using salts as the principal precipitating agents, were generally characterized by oiling out of protein and various other

manifestations of phase separation. This is a common result with lipophilic proteins and those with a propensity to form non-specific aggregates. Intact antibodies frequently show such tendencies and phase separation is the most serious obstacle to their crystallization (Kuznetsov *et al.*, 2001).

The screens were repeated at 295 K, but one of six different detergents was included in the protein droplets. None was added to the reservoir. The six detergents used are shown in Table 1 and were chosen based only on our own previous successes with other proteins. Upon repeating the screens in the presence of detergents, it was noted that microcrystals appeared in Crystal Screen trial No. 42 in the presence of two of the detergents, *n*-octyl-β-D-thiomaltoside and *n*-dodecyl-α-D-maltopyranoside. Trial No. 42 contains 4.0 *M* sodium formate pH 7.0. We then deployed three 24-well Cryschem plates (a total of 72 trials) with identical samples using 4.0 *M* sodium formate pH 7.0 in all wells and drops, but with a different detergent in each. These were the surfactants in Detergent Screens I, II and III. Thus, the secondary screen examined each of 72 different detergents against the only precipitant conditions observed to yield crystals, 4.0 *M* formate pH 7.0.

Numerous detergents produced protein crystals from the formate solutions, but certain crystals appeared larger and more promising than others. The best crystals, as judged by inspection using light microscopy, appeared from the Anapoe series X-305, X-405, 58 and 80, as well as Triton X-100. MEGA-9 and MEGA-8 also produced encouraging results.

Optimization trials were carried out in which the concentrations of sodium formate, pH, temperature, detergent and detergent concentration were varied. In the end, Anapoe X-405 and Triton X-100 were chosen as the optimal detergents. It was also found that the best crystals for both detergents were grown at 290 K. We observed in the course of optimization that the concentration of the detergent in 4.0 *M* formate which yielded the largest crystals was only slightly below the concentration at which the detergent itself formed microdroplets and emerged from solution. Results were noticeably sensitive to temperature and fluctuations were clearly deleterious to ultimate crystal quality.

In the end, large crystals of the antibody were grown from 4.0 *M* sodium formate pH 7.0 in the presence of 1.5 m*M* Anapoe X-405 or Triton X-100 at 290 K. The crystals grown in the presence of Anapoe X-405 were generally larger than those from Triton X-100. The former, shown in Fig. 1(*a*), were thick laths and plates, often greater than 0.4 mm in their longest dimension. Those from Triton X-100, seen in Fig. 1(*b*), were smaller and more needle-shaped, but nonetheless well formed.

A number of different cryogens were explored, as well as freezing of the crystals directly from their mother liquor. Crystals grown from Anapoe X-405 could not be frozen directly, but could be flash-frozen if briefly passed through a mixture of 50% MPD, 20% PEG 3350 and 1.5 *M* sodium formate pH 7.0. Crystals grown from Triton X-100, however, could be frozen directly from their mother liquor. Successful freezing was judged not only by the absence of ice rings but also by the appearance of an acceptable diffraction pattern.

Table 2
Crystal and data-collection statistics.

Values in parentheses are for the highest resolution shell.

Resolution (Å)	45.1–2.8 (2.9–2.8)
No. of observations	696849
No. of unique reflections	76929 (7574)
Redundancy	9.06
Completeness	99.87 (99.83)
$R_{\rm merge}$ on I	0.152 (0.365)
Normalized χ^2	0.91 (1.06)
Mean $I/\sigma(I)$	10.9 (5.0)
Space group	$P2_12_12$, $Z = 8$
Unit-cell parameters (Å)	$a = 83$, $b = 224$, $c = 167$

Preliminary X-ray diffraction data collected on the laboratory apparatus and on the synchrotron were consistent. The large morphologically attractive crystals grown in the presence of Anapoe X-405 produced only low-resolution and often disordered diffraction patterns, apparently twinned lattices and rapidly decaying patterns. This was true at both 295 and 100 K. They were morphologically attractive but in practice useless for analysis. Crystals grown in the presence of Triton X-100, on the other hand, despite producing weaker intensities because of their smaller size, yielded completely ordered diffraction patterns that extended beyond 2.8 Å resolution. Furthermore, reflections showed little decay over the course of high-redundancy data collection at 100 K. The diffraction patterns of crystals grown from Anapoe X-405 and Triton X-100 appeared to be similar, but it was difficult to confidently index the reflections from crystals grown from Anapoe X-405 or to assign a space group. Signs of disorder were persistently evident.

Data to 2.8 Å resolution collected at 100 K on beamline 5.0.2 at ALS from crystals grown from Triton X-100 were processed and merged to an R of 15% and an average redundancy of 9, with 99% completeness in the outermost (2.9–2.8 Å) shell. Data statistics are shown in Table 2. The symmetry of the reciprocal lattice and systematic absences were consistent with space group $P2_12_12$, with unit-cell parameters $a = 83$, $b = 224$, $c = 167$ Å. Assumption of two entire antibody molecules of 120 kDa as the asymmetric unit implies a unit cell volume-to-weight ratio, $V_{\rm M}$ (Matthews, 1968), of 3.2 Å^3 Da^{-1} and seems the most reasonable choice. It is also most consistent with the AFM results (see below).

We noted elsewhere (Kuznetsov *et al.*, 1997) that information complementary to X-ray diffraction can be obtained using AFM techniques. We attempted to employ that approach here. In Fig. 2, the 011 surfaces of crystals growing in the presence of Anapoe X-405 can be seen. On these surfaces toroid-shaped objects are adsorbed, with a depression in their centers, with outside diameters estimated to be about 150 Å and thicknesses of about 90 Å. An AFM image is the convolution of tip shape with object. Because the AFM tip is not infinitely sharp, lateral dimensions are significantly broadened. Hence, the toroids appear much broader than in reality. Height measurements, however, are accurate to less than 1 nm. From

AFM images of different surfaces of the crystals, it is evident that the toroids are the crystallizing units.

Measurements of the heights above background of the toroids on both crystal surfaces and the substrate plane indicate that the majority are about 90 Å in thickness, but occasionally rings are observed which are only half that height. The thickness of a single antibody molecule is roughly 45 Å (Harris *et al.*, 1998, 1999), suggesting that the rings are probably a circular dimer of two molecules. A toroid of 90 Å thickness, furthermore, would occupy a volume corresponding to four domain-deleted antibodies of M_r = 120 000 each. We therefore conclude that the toroidal objects are comprised of four molecules having a total M_r = 480 000 and that they have a double-ring structure. Crystallographic considerations would require that the toroids exhibit C_2 symmetry and that the dyad axis be directed along the *c* direction in the crystal. Thus, the two rings that form the toroid would have to be face to face and twofold related.

In crystals, the toroids are stacked, like plates, in columns that run along the *a* direction. Using AFM, we can measure the heights of growth steps (Malkin *et al.*, 1995, 1996; Kuznetsov *et al.*, 1997) on the 011 face, like those shown in Fig. 2. Because the rows of crystallization units in successive layers are stacked directly above one another, the steps provide a further and more accurate estimate of the diameter of the toroids since they depend only on height measurements. The steps are consistently about 150 ± 10 Å. The diameters of the toroids can also be estimated from the center-to-center distances of rows of toroids (or the furrows between them) running along *a*, seen in Fig. 3(*a*), and even more precisely from Fourier transforms and Fourier-filtered AFM images of a 011 surface, like that in Fig. 3(*b*). From the Fourier transform, the toroid diameters, consistent with the value from step-height measurements, are 150 Å.

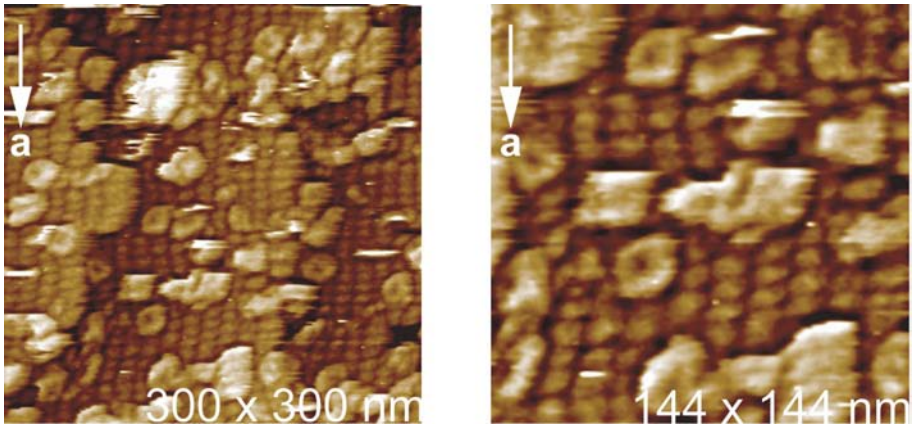

Figure 2
Atomic force micrographs in protein-free mother liquor of 011 surfaces of the antibody crystals fixed with glutaraldehyde. The surfaces are cluttered with molecular aggregates. It can be seen that many are toroidal in shape with a distinctive depression at their centers. These are the crystallizing units of the crystals and consist of four antibody molecules. Also present on both crystal surfaces and the substrate are rings of half the thickness of the toroids, composed of two antibody molecules. Toroidal aggregates incorporated into the crystal are viewed edge-on and are stacked like plates along the *a* direction, while those adsorbed to the surface have an orientation perpendicular to the crystal surface.

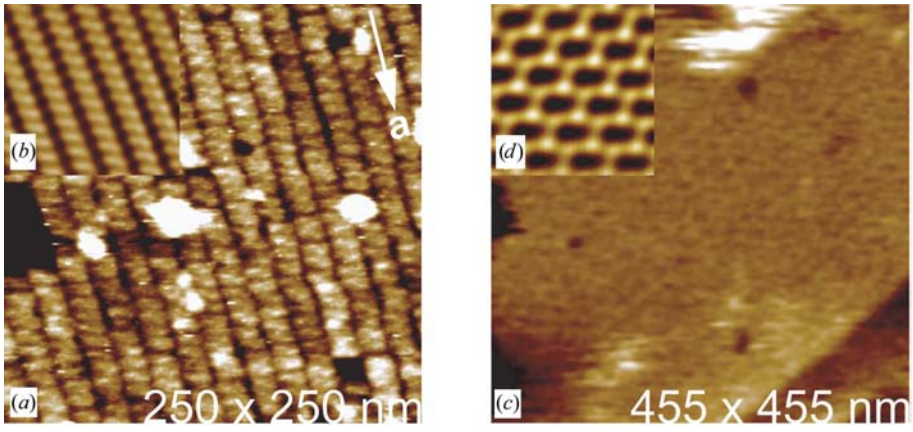

Figure 3
(*a*) An AFM image of the 011 surface of an antibody crystal where the view of the toroidal units is edge-on. The axes of the toroids are aligned along the *a* direction. (*b*) A Fourier-filtered image of the raw micrograph in (*a*). (*c*) A raw AFM image, at lower magnification, of the 110 face of a crystal, viewing the toroids along their axes. (*d*) A low-resolution Fourier-filtered image of the raw micrograph shown in (*c*).

It would have been informative to have visualized toroidal stacks end-on and thereby view the toroids along their axes, but this was problematic. The 100 plane is not a crystal face and the 110 plane, which is, is a prismatic face that is not generally accessible to the AFM tip. This is because of the difficulty of maintaining crystals fixed in an arbitrary orientation in a fluid cell. Nonetheless, some micrographs, such as that shown in Fig. 3(*c*), were obtained along with their corresponding Fourier-filtered image, as seen in Fig. 3(*d*). The elliptical cross-sections in the latter arise because the toroids are not parallel to the 110 surface, but are packed with a relative tilt of about 20°. Full step heights on this surface (there are also half step heights, see below) give a further estimate of the thickness of the toroids and were measured to be 90 Å.

Some other observations from the AFM images are pertinent to the crystallographic analysis. The growth of these antibody crystals, as seen in Fig. 4(*a*), proceeds by addition of layers using the mechanism of two-dimensional nucleation (Malkin *et al.*, 1995; McPherson *et al.*, 2000, 2001). No screw dislocations were observed. Advancement of step edges occurred by addition of the toroid units into kinks at the ends of rows along *a*. As seen in Fig. 4(*b*), the layers are riddled with point defects and absences and the step edges are extre-

mely rough and irregular, indicating a high level of impurity incorporation (Malkin *et al.*, 1996; McPherson *et al.*, 1996).

There are likely to be two major sources of impurities in the crystals. The antibody preparation used in growing the crystals contained a small but detectable level of the A form of the molecule which contains disulfide bonds in the hinge region. The A form of the molecule, which in most other ways resembles the B form, may compete for incorporation sites on the surfaces. It appears that in addition to the toroids of B-form molecules, there is also an abundance of various non-specific aggregates present in solution. These may also block sites at the step edges and serve as stoppers (Plomp *et al.*, 2003; Vekilov & Chernov, 2003). Such non-specific aggregation is consistent with the oiling out and phase separation that characterized mother liquors in the absence of detergent (Kuznetsov *et al.*, 2001).

In examining the AFM images of the surfaces of crystals grown from the Anapoe series of detergents, we noted an unusual growth-defect phenomenon that we have not seen in other protein crystals. It is likely to be a consequence of the double-ring toroidal nature of the crystallizing unit. In some images, as illustrated in Fig. 5(*a*), the lattice, looking from left to right, shifts up by half the thickness, ∼45 Å, of a toroidal unit (half a crystallographic lattice dimension along *a*). We observe no planar defects on the 011 plane, but do see steps of half the toroid height on the 110 plane. Thus, planar defects, such as those in Fig. 5(*b*), are formed by nucleation and growth of a new layer whose lattice is shifted half a unit-cell parameter along *a*.

Two kinds of steps are present on the 110 surfaces of the crystals: steps of full height (equal to a toroid thickness, ∼90 Å) and half steps. The latter are stationary and do not move with time, while full steps move over the surfaces producing new layers, *i.e.* they are the growth steps. The half steps on the 110 surface exhibit a polarity. For example, in Fig. 5(*b*) the step is always from a higher terrace to a lower terrace from left to right across the crystal. There is no mixture of half steps, some rising and others falling. The lower terraces on a surface are all always to the right or to the left. This can be explained if, as indicated in Fig. 6(*a*), toroidal units can only add on one side of a half step two-dimensional island, not on the other side. This is possible since the symmetry of the crystal does not pertain on the surface layer. Thus, asymmetric addition of molecules to the opposite edges of two-dimensional islands is common (for other examples, see Malkin *et al.*, 1995, 1996).

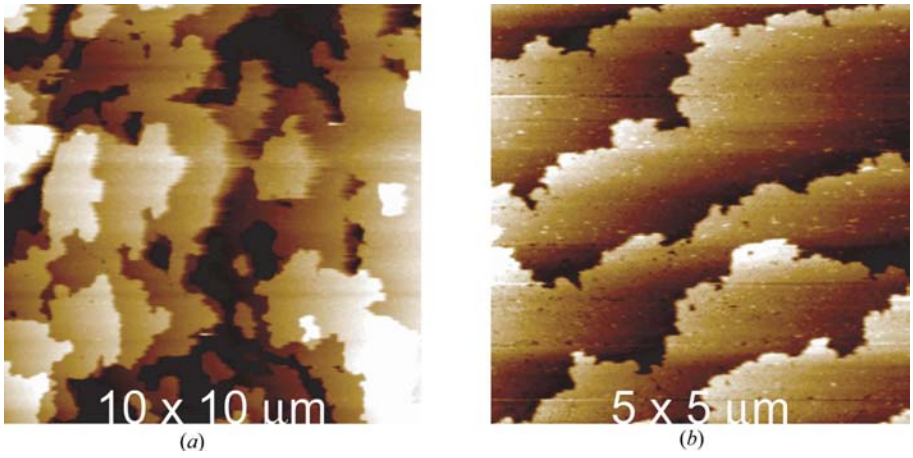

Figure 4
In these relatively low-resolution AFM images of an antibody crystal surface, sequential layers and their step edges can be seen. The layers are pocked with absences and the edges are unusually rough and irregular, certain indications of high levels of impurity incorporation.

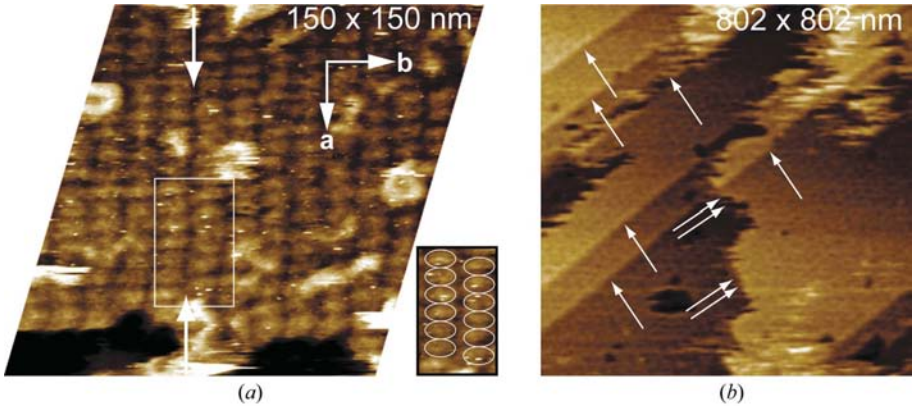

Figure 5
(*a*) The 001 surface of an antibody crystal containing a half-step shift between rows (top arrow), which in turn creates two mosaic blocks offset by half a lattice parameter along the *a* direction. An area exhibiting this shift plane, in the box outlined in white (lower arrow), is detailed at the lower right. Toroidal assemblies of antibodies are also seen *en face* that have sedimented on the surface. (*b*) Immobile half steps on the 110 planes are produced by the shift planes seen in (*a*) and are indicated by single arrows. Steps of full height which provide growth are indicated by double arrows.

In Fig. 6(*a*), on the active side of the half step where addition can take place, growth proceeds normally to the left, leaving a lower terrace to the right. Events proceed differently, however, for growth steps when they encounter the dormant side of a half step, depending on their direction of movement. As shown in Figs. 6(*b*), 6(*c*) and 6(*d*), when the growth-step edge moves on the upper terrace of the half step and ultimately reaches the edge of the half step, a new step one-and-a-half times the toroid dimension (∼135 Å) forms. Toroidal units continue to be incorporated into the growth-step edge at the one-and-a-half step kink site as shown in Figs. 6(*b*), 6(*c*) and 6(*d*). The half step is overgrown, but a half step exactly one lattice unit above is created. Thus, the position of the half step remains the same through all of the layers, creating a boundary between two mosaic blocks

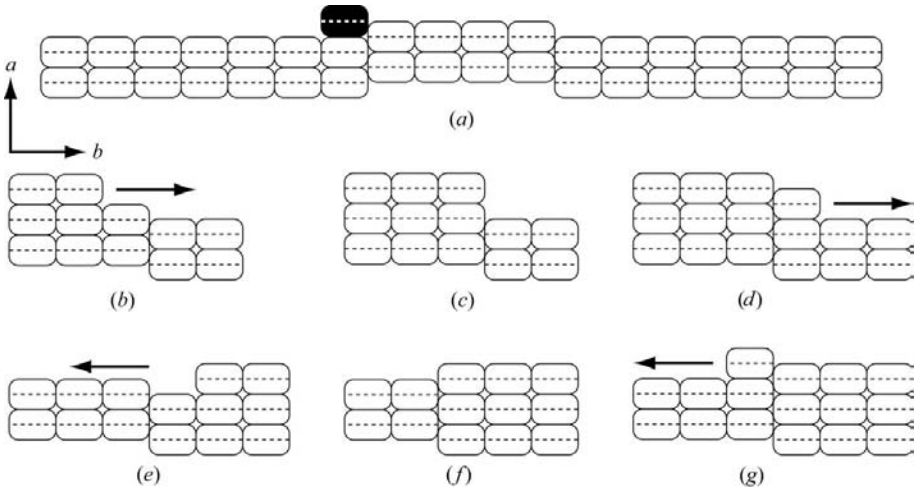

Figure 6
In (*a*) a molecule incorporates onto the active side of a half-step dislocation identified by atomic force microscopy. In (*b*), (*c*) and (*d*) the growth step approaches a half step along its upper terrace. In (*e*), (*f*) and (*g*) the growth step moves along the lower terrace and encounters the half-step edge straight on. In both cases, the half-step dislocation moves neither right nor left, but is propagated through successive growth layers.

which are displaced with respect to each other by half a lattice translation.

When a growth-step edge moves onto the lower terrace of the half step, as illustrated in Figs. 6(*e*), 6(*f*) and 6(*g*), and encounters the dormant half-step edge, then another half-step edge forms, again directly above the pre-existing one but of opposite orientation. Toroid units do incorporate into the half-step edge in this direction and new growth layers move forward, leaving the half-step edge behind. Again, two mosaic blocks displaced by half a lattice parameter result. No matter whether the half-step edges are overgrown by moving full step edges arising from two-dimensional islands on the right or left, the half steps remain stationary and the lower terrace maintains its orientation with respect to the higher terrace. There are a great many half steps in the crystal lattices of the Anapoe detergent-grown crystals. Thus, there must be close to a 1:1 mixture of domains throughout the lattice which are displaced with respect to one another by a translation of half a lattice parameter.

4. Discussion

This is one of the few intact monoclonal antibodies to be crystallized in a form suitable for X-ray diffraction analysis (Harris *et al.*, 1999), the first intact chimeric (human–murine) antibody and the first lacking a C_H2 domain or disulfide bonds in the hinge region. A somewhat unanticipated result of this preliminary analysis, which must await the structure determination for confirmation, is that the antibody apparently forms discrete symmetrical aggregates of unique structure composed of four molecules and that the toroidal tetramer, which is preformed in the mother liquor, is the unit of incorporation into the crystals.

Crystals grown in the presence of Anapoe X-405 display a unique kind of planar defect in which some layers are displaced with respect to those above or below by half the thickness of a tetrameric unit. This gives rise to a mosaic of domains throughout the crystals that are out of alignment by half a unit-cell parameter along *a*. These defects are frequent and no doubt contribute to the severe disorder of the X-ray diffraction patterns and the low resolution to which the crystals diffract.

Successful crystallization depended on the recognition that phase separation in the initial negative set of experiments implied non-specific aggregation. This was followed by retesting in the presence of a limited set of detergents which yielded the small breakthrough which, when pursued by application of a broader detergent screen, ultimately gave crystals suitable for analysis. It is noteworthy that the quality of the crystals obtained in this investigation was acutely dependent on which detergent was present, as was the ability to flash-freeze the crystals. The impact of the detergent was particularly pronounced since the Anapoe series of detergents, which yielded disordered crystals, are also members of the Triton detergent class. However, only Triton X-100 gave highly ordered crystals. The concentration of Triton X-100 in the mother liquor was nearly 100 times the CMC. This is many times that usually assumed necessary in crystallization. It seems to suggest that a significant excess of detergent is not necessarily detrimental. The results obtained here again demonstrate the critical role that detergents play in determining lattice interactions and defect structure.

The value of atomic force microscopy as a complement to X-ray crystallography has again been demonstrated. Without the AFM images there would be no knowledge of the composition and structure of the asymmetric unit, the unit of crystallization or the precrystallization form of the molecules or any explanation of the disorder found in some crystals and the sources of the unusually high defect density and the consequent poor diffraction qualities of the Anapoe-grown crystals.

This research was supported by NIH grant GM58868-02 and contracts from NASA. The authors wish to thank Mr Aaron Greenwood for assistance in preparing the figures.

References

Braslawsky, G. R., Hanna, N. & Chinn, P. (2003). *Modified Antibodies and Method of Use.* US Patent.

Calvo, B., Kashmiri, S. V., Hutzell, P., Hand, P. H., Slavin-Chiorini, D. C., Schlom, J. & Zaremba, S. (1993). *Cancer Biother. Radiopharm.* **8**, 95–109.

Harris, L. J., Larson, S. B. & McPherson, A. (1999). *Adv. Immunol.* **72**, 191–208.
Harris, L. J., Larson, S. B., Skaletsky, E. & McPherson, A. (1998). *Immunol. Rev.* **163**, 35–43.
Kabat, E. A., Wu, T. T., Perry, H., Gottesman, K. & Foeller, C. (1991). *Sequences of Proteins of Immunological Interest.* Bethesda, MD, USA: NIH Publications.
Kuznetsov, Y. G., Malkin, A. J., Land, T. A., DeYoreo, J. J., Barba, A. P. & McPherson, A. (1997). *Biophys. J.* **72**, 2357–2364.
Kuznetsov, Y. G., Malkin, A. J. & McPherson, A. (2001). *J. Cryst. Growth*, **232**, 30–39.
McPherson, A. (1999). *Crystallization of Biological Macromolecules*. Cold Spring Harbor, New York: Cold Spring Harbor Laboratory Press.
McPherson, A., Malkin, A. J. & Kuznetsov, Y. G. (2000). *Annu. Rev. Biophys. Biomol. Struct.* **29**, 361–410.
McPherson, A., Malkin, A., Kuznetsov, Y. G. & Koszelak, S. (1996). *J. Cryst. Growth*, **168**, 74–92.
McPherson, A., Malkin, A. J., Kuznetsov, Y. G. & Plomp, M. (2001). *Acta Cryst.* D**57**, 1053–1060.
Malkin, A. J., Kuznetsov, Y. G., Land, T. A., DeYoreo, J. J. & McPherson, A. (1995). *Nature Struct. Biol.* **2**, 956–959.
Malkin, A. J., Kuznetsov, Y. G. & McPherson, A. (1996). *J. Struct. Biol.* **117**, 124–137.
Matthews, B. W. (1968). *J. Mol. Biol.* **33**, 491–497.
Mueller, B. M., Reisfeld, R. A. & Gillies, S. D. (1990). *Proc. Natl Acad. Sci. USA*, **87**, 5702–5705.
Otwinowski, Z. & Minor, W. (1997). *Methods Enzymol.* **276**, 307–326.
Pflugrath, J. W. (1999). *Acta Cryst.* D**55**, 1718–1725.
Plomp, M., McPherson, A. & Malkin, A. J. (2003). *Proteins*, **50**, 486–495.
Slavin-Chiorini, D. C., Kashmiri, S. V., Lee, H. S., Milenic, D. E., Poole, D. J., Bernon, E., Schlom, J. & Hand, P. H. (1997). *Cancer Biother. Radiopharm.* **12**, 305–316.
Slavin-Chiorini, D. C., Kashmiri, S. V., Schlom, J., Calvo, B., Shu, L. M., Schott, M. E., Milenic, D. E., Snoy, P., Carrasquillo, J. & Anderson, K. (1995). *Cancer Res.* **55**, 5957–5967.
Vekilov, P. G. & Chernov, A. A. (2003). *Solid State Phys.* **57**, 1–147.